The Next-Generation Energy Storage System Using a Cascade PWM Converter with Star Configuration

Hirofumi Akagi, *Fellow, IEEE*
Department of Electrical and Electronic Engineering
Tokyo Institute of Technology, Tokyo, Japan
E-mail: akagi@ee.titech.ac.jp

***Abstract*— This paper describes the next-generation 6.6-kV transformerless energy storage system based on a cascade multi-level PWM converter with star configuration. The system is intended to make power systems reliable and efficient, as well as to improve power quality. The paper pays attention to active-power control and voltage-balancing control that are indispensable for proper operation of the energy storage system. A 200-V, 10-kW, 8.8-kJ downscaled laboratory system is designed, constructed, and tested, replacing EDLCs (electric double layer capacitors) with large-capacity electrolytic capacitors. Experimental results obtained from the laboratory system verify the viability and effectiveness of the 6.6-kV energy storage system.**

***Index Terms*— Active-power control, cascade PWM converter, EDLC, energy storage system, voltage-balancing control.**

I. Introduction

Energy storage systems can level uneven active-power flow, improve transient and dynamic stability, and make power systems reliable [1]-[9]. Power quality can be significantly improved by storing electrical energy from the grid or delivering it to the grid, as and when it is required, in a range of a few seconds up to a minute.

There are three major static energy storage devices; batteries, superconducting magnetic coils, and EDLCs (electric double layer capacitors) [10]-[13]. Although leading-edge Li (lithium)-ion batteries offer better energy densities and increased cycling capabilities, they are not yet cost-effective for high-power applications at present. Moreover, design engineers face the challenge to overcome poor low-temperature performance and limited lifetime. SMES (superconducting magnetic energy storage) systems [14][15] have high efficiency and fast response capability. However, the overall system is costly for short-term energy storage applications, because the refrigerating unit as well as the magnetic coils is complex and expensive.

In an area of energy storage, the EDLC is emerging as a promising device [16][17]. It provides a simple solution to buffer a short-term mismatch in active power between supply and demand. An EDLC bank has a specific energy density of 5 Wh/kg and a specific power density of up to 20 kW/kg. Recent advances in EDLCs has made it suitable to put them into short-term high-power energy storage applications at reasonable cost.

However, since a single EDLC-cell voltage is as low as around 2.5 V, many cells connected in series are required to reach a desirable EDLC-bank voltage. Many EDLC cells with unequal capacitance values might lead to cell-voltage imbalance because a common dc current flows through the series-connected EDLC cells. This problem can be mitigated by replacing a traditional two-level converter with a modern multi-level converter. The use of the multi-level converter makes individual EDLC-bank voltages low with easy series connection of EDLC cells. Besides, its transformerless circuit structure allows direct connection to a medium-voltage grid with less voltage/current harmonics without bringing any increase in voltage rating to individual switching devices.

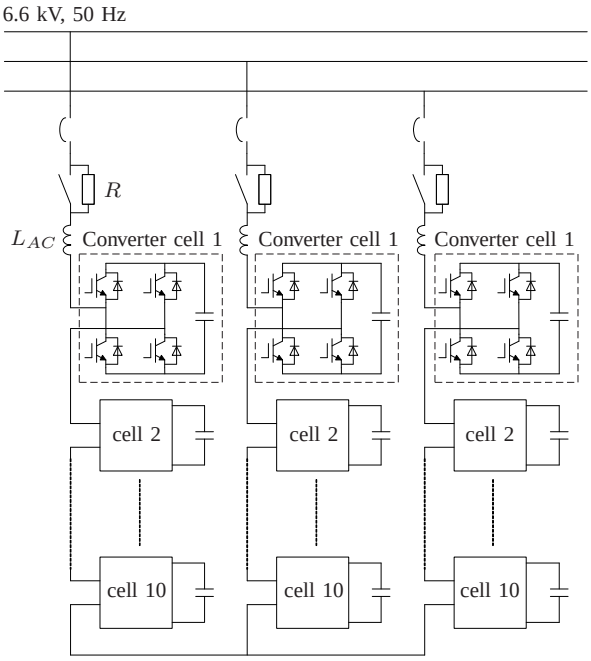

Fig. 1. Feasible circuit configuration of the 6.6-kV, 1-MW transformerless energy storage system based on a cascade multi-level PWM converter using 120 IGBTs rated at 1.2 kV and 200 A.

The goal of this research project is to realize the 6.6-kV transformerless energy storage system based on a cascade mulit-level PWM (pulsewidth modulation) converter with star configuration. The authors of [18] presented a motor drive system based on a cascade multi-level SCM (staircase modulation) converter. However, unequal converter losses and/or background harmonic and negative-sequence voltages might make individual dc voltages unbalanced. This problem would get more prominent when the converter absorbs an active power from the grid, or releases it to the grid.

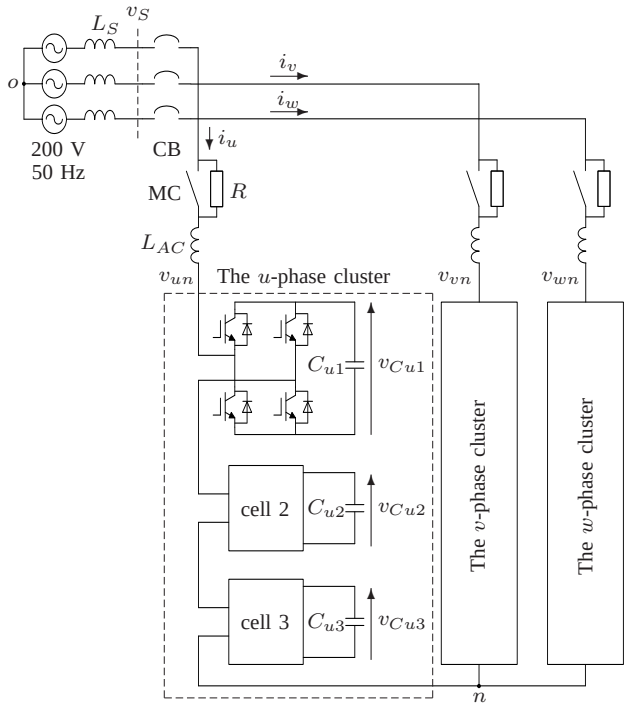

Fig. 2. Experimental system configuration of the 200-V, 10-kW, 8.8-kJ downscaled energy storage system with a cascade number of $N = 3$.

TABLE I
CIRCUIT PARAMETERS OF THE EXPERIMENTAL SYSTEM RATED ON 200 V, 10 KW AND 50 HZ.

Nominal line-to-line rms voltage	V_S	200 V
Power rating	P	10 kW
Cascade number	N	3
AC inductor	L_{AC}	1.2 mH (10%)
Background system inductance	L_S	48 μH (0.4%)
Starting resistor	R	10 Ω (250%)
DC voltage	V_C	65 ∼ 80 V
DC capacitor	C	0.9 F
Unit capacitance constant [20]	H	2.6 s at 80 V
PWM carrier frequency		1 kHz
Equivalent carrier frequency		6 kHz

on a three-phase, 200-V, 10-kW, 50-Hz base

This paper addresses voltage-balancing control for the energy storage system based on the cascade multi-level PWM converter, with focus on a design procedure of control gains and parameters. Star configuration is chosen instead of delta configuration so as to minimize the number of converter cells connected in cascade. However, star configuration makes voltage-balancing control much more complicated than delta configuration. Experimental results obtained from a three-phase, 200-V, 10-kW, 8.8-kJ laboratory model using large-capacity electrolytic capacitors confirm the feasibility of the 6.6-kV energy storage system.

II. DESIGN CONCEPT OF THE 6.6-KV SYSTEM

Fig. 1 shows the 6.6-kV energy storage system using EDLCs. This system is based on the cascade connection of 10 single-phase H-bridge PWM converter cells per phase. The

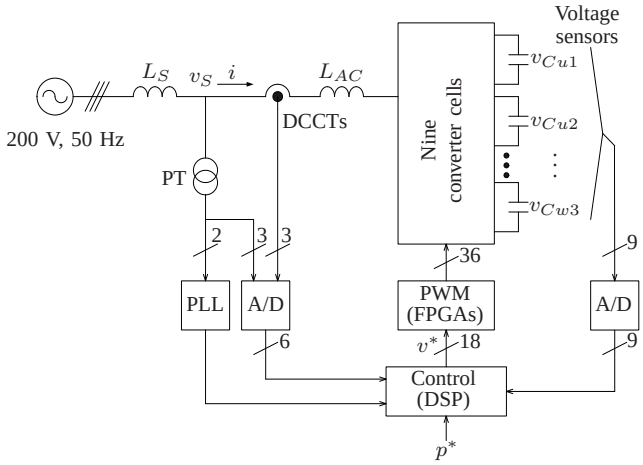

Fig. 3. Control system for the 200-V energy storage system.

so-called “asymmetrical cascade converter” with binary-scale EDLC-bank voltages might be attractive in lower harmonics and reduced switching loss [19]. The authors of this paper, however, prefer the symmetrical cascade converter to the asymmetrical cascade converter in terms of having the same EDLC-bank voltage. The ac voltage of each converter cell is $6,600/10\sqrt{3} = 381$ V. This allows the use of 1.2-kV IGBTs (insulated-gate bipolar transistors) that are available on the market at reasonable cost. The maximal EDLC-bank voltage would be limited to about 750 V from a practical point of view, because a higher-voltage EDLC bank has difficulty in achieving voltage balancing of many series-connected EDLC cells. The ac voltage cascaded results in a 21-level waveform in line-to-neutral, and a 41-level waveform in line-to-line. When a PWM carrier frequency is as low as 1 kHz, the use of the so-called “phase-shifted unipolar sinusoidal PWM” makes an equivalent carrier frequency as high as 20 kHz. Moreover, setting such a low carrier frequency as 1 kHz brings a significant reduction in switching power loss to each converter cell.

III. THE 200-V, 10-KW, 8.8-KJ DOWNSCALED SYSTEM

Fig. 2 shows the system configuration of a three-phase downscaled energy storage system rated at 200 V, 10 kW and 8.8 kJ. Table I summarizes the circuit parameters. Nine electrolytic capacitors, each of which is rated at 100 V and 0.9 F, are used, instead of EDLCs. The capacitance of the capacitor, C [F] gives its available energy W [J] as follows:

$$W = \frac{1}{2}C(V_{Cmax}^2 - V_{Cmin}^2), \quad (1)$$

where V_{Cmax} [V] and V_{Cmin} [V] are the maximal and minimal capacitor voltages. The difference between the maximal and minimal voltages, $\Delta V_C = V_{Cmax} - V_{Cmin}$ is typically around 20% of V_{Cmax} when the electrolytic capacitor is directly connected to the dc side of each converter cell without any bi-directional dc chopper.

The experimental system has a cascade number of $N = 3$, and the dc voltage is allowed to range between 65 and 80 V. The nine H-bridge converter cells are controlled by the phase-shifted unipolar sinusoidal PWM with a carrier frequency of

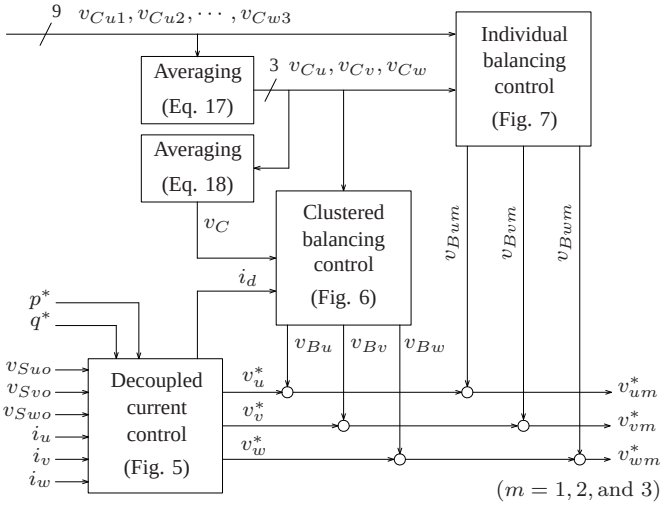

Fig. 4. Control block diagram for the 200-V energy storage system.

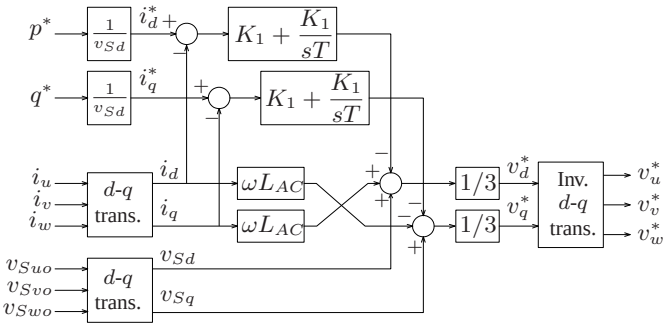

Fig. 5. Decoupled current control.

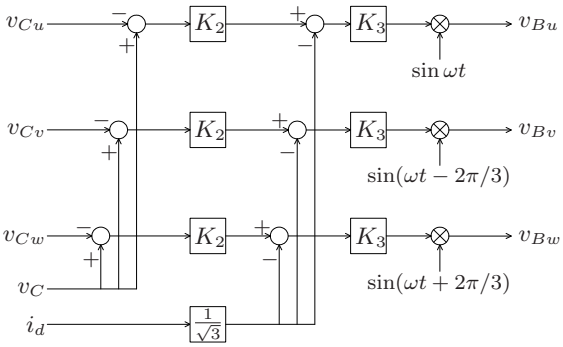

Fig. 6. Clustered balancing control between the u-phase, the v-phase and the w-phase clusters, where each of the three clusters is considered as a single-phase H-bridge converter cell using four IGBTs.

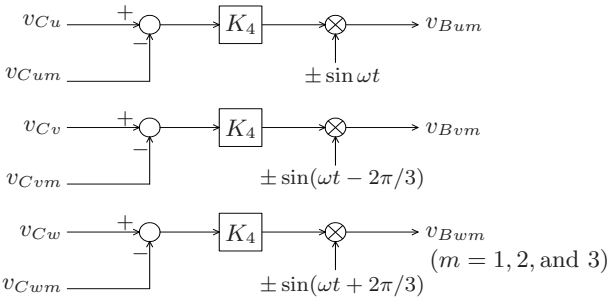

Fig. 7. Individual balancing control between three cascaded converter cells inside each cluster, paying attention to the m^{th}-converter cells.

1 kHz. The resulting line-to-neutral voltage is a seven-level waveform with an equivalent carrier frequency of 6 kHz. An ac inductor L_{AC} $(= 10\%)$ in each phase supports the difference between the ac grid voltage and the seven-level PWM voltage. It also helps in filtering out switching voltage/current ripples caused by PWM.

Fig. 3 shows the control system of the 200-V, 10-kW energy storage system. This is based on a fully-digital controller using a DSP (digital signal processor) and multiple FPGAs (field programmable gate arrays).

IV. Control Strategy

Fig. 4 shows the control block diagram of the 200-V energy storage system. The whole control is divided into the following two sub-controls:

1) decoupled current control of independent active and reactive power, and
2) voltage-balancing control of all the nine electrolytic capacitors.

Moreover, the voltage-balancing control is divided into "clustered balancing control" between the three clusters, and "individual balancing control" between three cascaded converter cells in each cluster. Although the control system is similar to that presented in [21], the following difference exists: This system is an energy storage system for active-power control, whereas the system in [21] is a STATCOM for reactive-power control. The cascade multi-level PWM converter used as a STATCOM can control reactive power without causing any voltage imbalance in an ideal condition. This is because the capacitor voltages are balanced by equal charge and discharge in each half cycle. This is, however, not the case when the cascade multi-level PWM converter is used as an energy storage system. In a real system, voltage imbalance always appears due to unequal power losses and/or component tolerances in the converter cells. Continuous and repetitive absorption or release of active power brings more serious voltage imbalance to the converter cells.

Since the overall dc mean voltage in this system varies with absorbing or releasing active power, the dc voltage control presented in [21] no longer exists in this system. The voltage-balancing controllers for the energy storage system and the STATCOM, however, resemble each other in structure except for the aforementioned differences.

Fig. 8 illustrates the sampling method for the downscaled model. For the sake of simplicity, attention is paid to one of the three clusters. Although each cluster has three carrier signals with the same carrier frequency as 1 kHz, they are phase-shifted by $2\pi/3$. Data sampling, for example, for converter cell 1 is carried out at every peak or trough of the carrier signal for converter cell 2. The corresponding voltage reference is

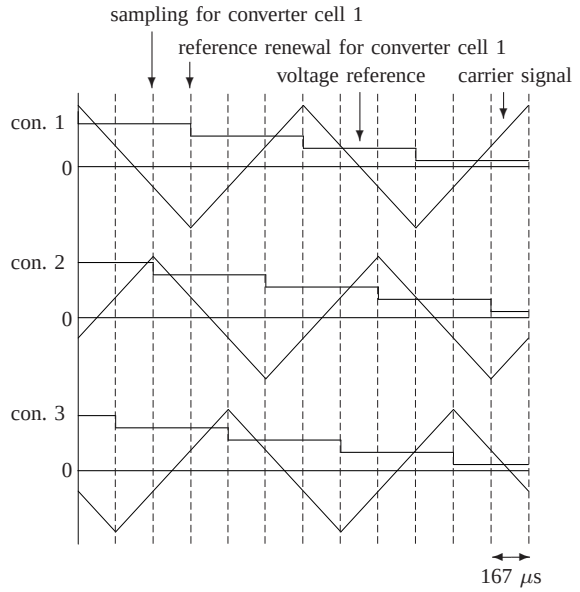

Fig. 8. Sampling method showing three phase-shifted carriers and three reference signals for a cluster of three converter cells of one phase.

renewed at the following peak or trough of the carrier signal for converter cell 1 with a time delay of 167 μs. It is held for 500 μs in order to avoid multi-switching. The equivalent carrier frequency results in 6 kHz $(= 1 \text{ kHz} \times 2 \times 3)$.

V. Decoupled Current Control

Referring to Fig. 2, along with neglecting the resistance components, gives the following set of voltage-current equations,

$$\begin{bmatrix} v_{Suo} \\ v_{Svo} \\ v_{Swo} \end{bmatrix} - \begin{bmatrix} v_{un} \\ v_{vn} \\ v_{wn} \end{bmatrix} = L_{AC} \frac{d}{dt} \begin{bmatrix} i_u \\ i_v \\ i_w \end{bmatrix}, \tag{2}$$

where

$$\begin{bmatrix} v_{Suo} \\ v_{Svo} \\ v_{Swo} \end{bmatrix} = \sqrt{\frac{2}{3}} V_S \begin{bmatrix} \sin \omega t \\ \sin(\omega t - \frac{2\pi}{3}) \\ \sin(\omega t + \frac{2\pi}{3}) \end{bmatrix}. \tag{3}$$

Applying the $d-q$ transformation leads to

$$\begin{bmatrix} L_{AC}\frac{d}{dt} & -\omega L_{AC} \\ \omega L_{AC} & L_{AC}\frac{d}{dt} \end{bmatrix} \begin{bmatrix} i_d \\ i_q \end{bmatrix} = \begin{bmatrix} v_{Sd} - v_d \\ v_{Sq} - v_q \end{bmatrix}, \tag{4}$$

where v_d and v_q are the *d*-axis and *q*-axis components of $\vec{v}$, while i_d and i_q are those of $\vec{i}$. Likewise, v_{Sd} and v_{Sq} are the d-axis and q-axis components of $\vec{v}_S$. The instantaneous active power *p* and the instantaneous reactive power *q* [22][23] can be expressed as

$$\begin{bmatrix} p \\ q \end{bmatrix} = \begin{bmatrix} v_{Sd} & v_{Sq} \\ -v_{Sq} & v_{Sd} \end{bmatrix} \begin{bmatrix} i_d \\ i_q \end{bmatrix}. \tag{5}$$

When the three-phase source voltages are balanced on the grid, v_{Sq} is always zero because $\vec{v}_S$ is aligned with the *d*-axis.

$$p = v_{Sd} i_d \tag{6}$$

$$q = v_{Sd} i_q. \tag{7}$$

Equations (6) and (7) imply that *p* and *q* can be controlled independently as a result of controlling i_d and i_q respectively. The d-axis current command i_d^* and the q-axis current command i_q^* are given by

$$i_d^* = \frac{p^*}{v_{Sd}} \tag{8}$$

$$i_q^* = \frac{q^*}{v_{Sd}} = 0, \tag{9}$$

where p^* is the active-power command, while the reactive power command of $q^* = 0$ ensures unity power-factor operation. Let the ac voltage commands in the *d*-axis and the *q*-axis be

$$\begin{bmatrix} v_d^* \\ v_q^* \end{bmatrix} = \frac{1}{3} \left(\begin{bmatrix} v_{Sd} \\ 0 \end{bmatrix} - \begin{bmatrix} 0 & -\omega L_{AC} \\ \omega L_{AC} & 0 \end{bmatrix} \begin{bmatrix} i_d \\ i_q \end{bmatrix} - K_1 \begin{bmatrix} i_d^* - i_d \\ i_q^* - i_q \end{bmatrix} - \frac{K_1}{T_1} \int \begin{bmatrix} i_d^* - i_d \\ i_q^* - i_q \end{bmatrix} dt \right). \tag{10}$$

The first and second terms on the right-hand side of (10) are introduced to cancel out the effect of the source voltage and the steady-state voltage appearing across the ac inductor L_{AC}. The third and fourth terms form a proportional-plus-integral (PI) controller with a proportional gain K_1 and an integral time constant T_1. Substituting (10) into (4) results in

$$\frac{d}{dt} \begin{bmatrix} i_d \\ i_q \end{bmatrix} = \frac{1}{L_{AC}} \begin{bmatrix} K_1(i_d^* - i_d) + \frac{K_1}{T_1} \int (i_d^* - i_d) dt \\ K_1(i_q^* - i_q) + \frac{K_1}{T_1} \int (i_q^* - i_q) dt \end{bmatrix}. \tag{11}$$

Equation (11) signifies that i_d and i_q can be controlled independent of each other. The three-phase reference signals v_u^*, v_v^* and v_w^* are obtained by applying the inverse *d*-*q* transformation to (10).

Fig. 9 shows the block diagram of the d-axis current control obtained by taking the Laplace transformation of (4) and (10). The transfer function can be determined as

$$\frac{I_d(s)}{I_d^*(s)} = \frac{K_1(sT_1 + 1)}{L_{AC}T_1 s^2 + K_1 T_1 s + K_1}. \tag{12}$$

Note that the one-sampling delay is neglected from (12). The damping ratio ζ is given by

$$\zeta = \frac{1}{2}\sqrt{\frac{K_1 T_1}{L_{AC}}}. \tag{13}$$

Setting $\zeta = 1$ leads to a critically-damped response,

$$K_1 = \frac{4L_{AC}}{T_1} = 0.5 \text{ V/A at } T_1 = 10 \text{ ms}. \tag{14}$$

The time constant T_1 should be assigned to be much longer than the control delay from the viewpoint of control stability.

VI. Voltage-Balancing Control

As shown in Fig. 4, the voltage-balancing control is divided into clustered balancing control and individual balancing control.

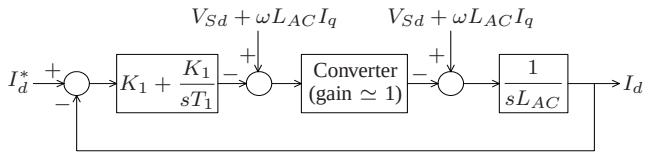

Fig. 9. Block diagram of the d-axis current control, excluding the effect of a one-sampling delay.

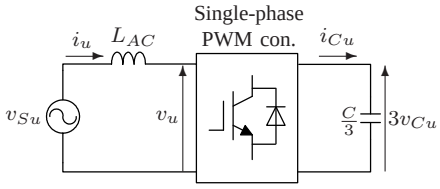

Fig. 10. Equivalent circuit to cascade connection of three single-phase converter cells in a cluster, taking u-cluster as an example.

A. Clustered Balancing Control

Fig. 6 shows the clustered balancing control. The aim is to keep the dc mean voltage of three cascade converter cells in each cluster equal to the dc mean voltage of the three clusters. The clustered balancing control considers a cluster of three single-phase cascaded converter cells in each phase as a single-phase PWM converter cell with a dc capacitor of $C/3$, as shown in Fig. 10. If the power loss within the converter cell is assumed negligibly small, the following approximation holds

$$v_{Su}i_u \simeq 3v_{Cu}i_{Cu}. \tag{15}$$

Let Δv_{Cu} be the difference between the dc mean voltage of the three clusters, v_C and the dc mean voltage of the u-cluster, v_{Cu}.

$$\Delta v_{Cu} = v_C - v_{Cu} \tag{16}$$

$$v_C = \frac{1}{3}\left(v_{Cu} + v_{Cv} + v_{Cw}\right) \tag{17}$$

$$v_{Cu} = \frac{1}{3}(v_{Cu1} + v_{Cu2} + v_{Cu3}). \tag{18}$$

The clustered balancing control produces the u-phase balancing signal v_{Bu} as

$$v_{Bu} = K_3\left(K_2\Delta v_{Cu} - \frac{i_d}{\sqrt{3}}\right)\sin\omega t, \tag{19}$$

where Δv_{Cu} and i_d are both dc signals. Multiplying the dc output signal from the minor current loop by "$\sin\omega t$" converts it into the ac signal being in phase, or out-of-phase by $180°$,

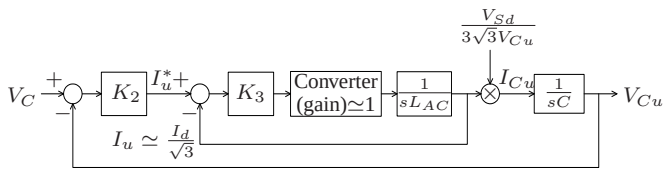

Fig. 11. Clustered balancing control, taking u-phase as an example.

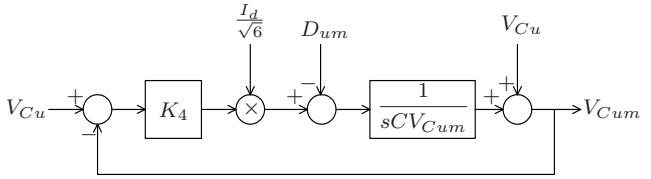

Fig. 12. Individual balancing control, taking u-phase m^{th}-converter cell as an example.

with ac output signal v_u^* from the decoupled current control. For v- and w-phases, $\sin\omega t$ is replaced by $\sin(\omega t - 2\pi/3)$ and $\sin(\omega t + 2\pi/3)$, respectively.

Fig. 11 shows the block diagram of the clustered balancing control, taking u-phase as an example. The inner loop forms a current controller with a transfer function of

$$\frac{I_u(s)}{I_u^*(s)} = \frac{K_3}{sL_{AC} + K_3}. \tag{20}$$

This transfer function is a first-order system with a time constant of

$$T_3 = \frac{L_{AC}}{K_3}. \tag{21}$$

The gain K_3 can be determined as

$$K_3 = \frac{L_{AC}}{T_3} = 0.06 \text{ V/A at } T_3 = 20 \text{ ms}. \tag{22}$$

The overall transfer function is given by

$$\frac{V_{Cu}(s)}{V_C(s)} = \frac{K_2K_3V_{Sd}}{s^2 3\sqrt{3}L_{AC}CV_{Cu} + s3\sqrt{3}K_3CV_{Cu} + K_2K_3V_{Sd}}. \tag{23}$$

The damping ratio ζ is given by

$$\zeta = \frac{1}{2}\sqrt{\frac{3\sqrt{3}K_3CV_{Cu}}{K_2L_{AC}V_{Sd}}}. \tag{24}$$

Taking $\zeta = 1$ leads to

$$K_2 = \frac{3\sqrt{3}K_3CV_{Cu}}{4L_{AC}V_{Sd}} = 19 \text{ A/V}. \tag{25}$$

B. Individual Voltage Balancing

Fig. 7 shows the block diagram of the individual balancing control. The aim is to keep each of the three dc voltages in each cluster equal to the dc mean voltage of the corresponding cluster.

Let Δv_{Cum} be the difference between the dc mean voltage of the u-cluster, v_{Cu} and the dc voltage of the m^{th}-converter cell in the u-cluster, v_{Cum}.

$$\Delta v_{Cum} = v_{Cu} - v_{Cum}, \tag{26}$$

where $m = 1$, 2, and 3. The compensating voltage to minimize Δv_{Cum} can be expressed as

$$v_{Bum} = \begin{cases} K_4\Delta v_{Cum}\sin\omega t & p^* > 0 \\ -K_4\Delta v_{Cum}\sin\omega t & p^* < 0. \end{cases} \tag{27}$$

TABLE II
CONTROL GAINS AND PARAMETERS.

	Analysis	Experiment
K_1	0.5 V/A	0.5 V/A
T_1	10 ms	10 ms
K_2	19 A/V	18.2 A/V
K_3	0.06 V/A	0.056 V/A
T_3	20 ms	21 ms
K_4	0.6 V/V	0.5 V/V
T_4	5 s	6 s

Equation (27) means that the individual balancing controller has a proportional gain of K_4.

Assuming $i_d >> i_q$, the *u*-phase current would be

$$i_u \simeq \sqrt{\frac{2}{3}} I_d \sin \omega t. \tag{28}$$

The active power for dc-voltage balancing of the u-phase m^{th}-converter cell can be written as

$$\begin{aligned} p_{Bum} &= v_{Bum} i_u - D_{um} \\ &= \frac{K_4 \Delta v_{Cum} I_d}{\sqrt{6}} (1 - \cos 2\omega t) - D_{um}, \end{aligned} \tag{29}$$

where D_{um} represents the loss or disturbance in the u-phase m^{th}-converter cell.

$$\Delta v_{Cum} \simeq -\frac{1}{C} \int \frac{p_{Bum}}{v_{Cu}} dt. \tag{30}$$

Equations (26), (29) and (30) result in the block diagram of the individual balancing control as shown in Fig. 12. The closed-loop transfer function is given by

$$\frac{\Delta V_{Cum}(s)}{D_{um}(s)} = \frac{1}{sCV_{Cu} + \frac{K_4 I_d}{\sqrt{6}}}. \tag{31}$$

This transfer function has the time constant given by

$$T_4 = \frac{C\sqrt{6} V_{Cu}}{K_4 I_d}. \tag{32}$$

Finally, the gain K_4 would be

$$K_4 = \frac{C\sqrt{6} V_{Cu}}{T_4 I_d} = 0.6 \text{ V/V at } T_4 = 5 \text{ s}. \tag{33}$$

The authors have designed the clustered balancing control to be much faster in response speed than the individual balancing control, because the clustered balancing control can be considered as a current controller whereas the individual balancing control as a voltage controller.

VII. EXPERIMENTAL RESULTS

A. Experimental Waveforms

Table II compares the control gains and parameters obtained from the analysis achieved in sections V and VI with those used in the following experiments.

Fig. 13 shows the experimental waveforms when the capacitor bank was charged up at the rated power of 10 kW. Although a small amount of 100-Hz component was superimposed on each dc-capacitor voltage, all the nine dc mean voltages remained balanced. The waveforms of v_{Suo} and i_u were in phase, because this system was operated with a condition of $q^* = 0$. The u-phase current was slightly distorted with a THD (total harmonic distortion) of 3.3%.

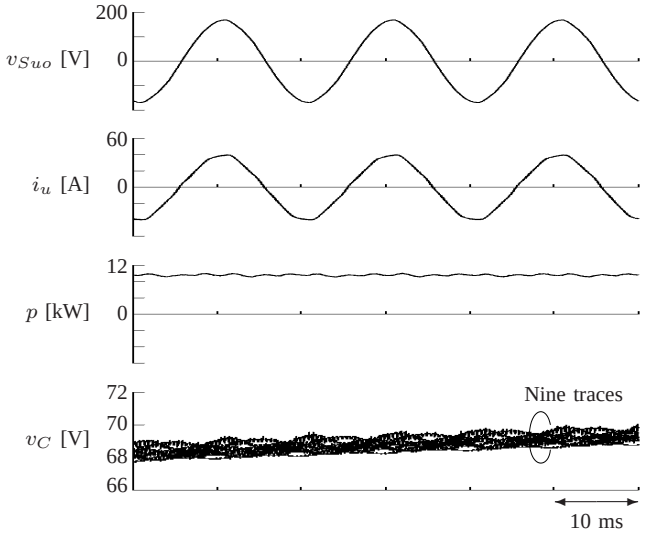

Fig. 13. Experimental waveforms when the capacitor bank was charged at 10 kW.

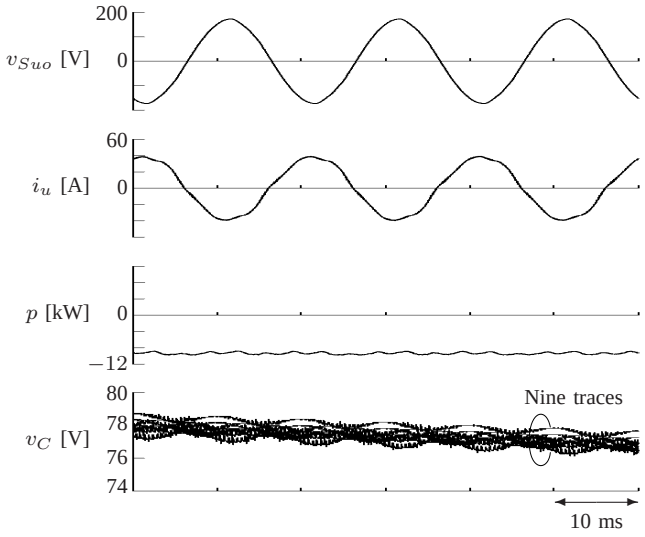

Fig. 14. Experimental waveforms when the capacitor bank was discharged at 10 kW.

Fig. 14 shows the experimental waveforms when the capacitor bank was discharged down at the rated power of 10 kW. The nine dc-capacitor voltages were balanced well. The waveforms of v_{Suo} and i_u were out of phase by 180°. In contrast to a THD of 3.3% during charging, the u-phase current had a THD of 5% during discharging. These THD values obtained from the experimental system would not be the case in an actual system. The reason is that this experimental system uses 36 IGBTs rated at 600 V and 150 A, each of which is integrated with a free-wheeling diode. The saturation voltage of the IGBT, $V_{CE(Sat)}$, and the forward voltage of the diode, V_F (both are about 1.5 V) produced a bad effect on current-control performance because the dc-capacitor voltage

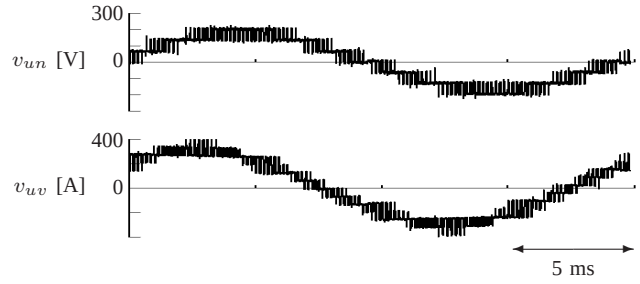

Fig. 15. Seven-level line-to-neutral and 13-level line-to-line voltage waveforms of the 200-V energy storage system.

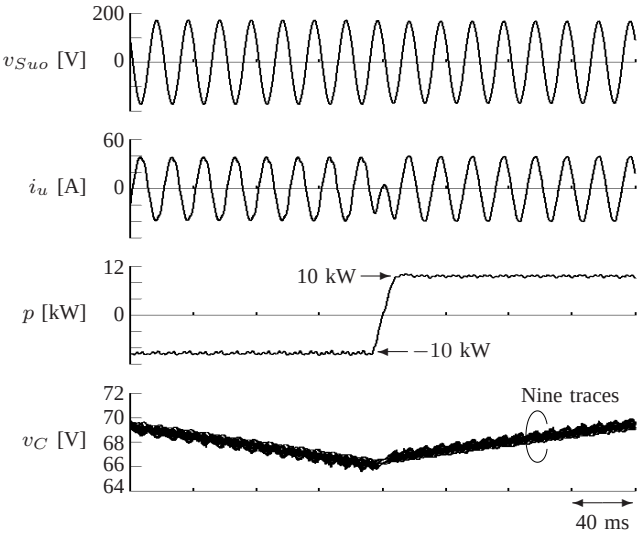

Fig. 16. Experimental waveforms when the active-power command p^* was changed from -10 kW to 10 kW in 20 ms, where the reactive-power command of $q^* = 0$.

ranged from 65 to 80 V. However, the dc voltage would range from 600 to 750 V in the actual system with a cascade number of $N = 10$, and a saturation/forward voltage of around 2.0 V in the latest 1.2-kV IGBTs would be only 0.3% of the dc voltage. This consideration, together with an increased number of voltage levels in the 6.6-kV system, results in a much lower current THD value.

Fig. 15 shows that the u-phase cluster voltage with respect to the neutral point n, v_{un} looks a seven-level waveform, and the u-phase cluster voltage with respect to the v-phase cluster voltage, v_{uv} looks a 13-level waveform as expected.

Fig. 16 shows transient waveforms from discharging to charging operation with a ramp change from -10 kW to 10 kW in 20 ms. Fig. 17 shows the experimental waveforms when the capacitor bank was repetitively charged up to 80 V and discharged down to 65 V. The total amount of energy charged into the capacitor bank was 9 kJ $(= 10\ \text{kW} \times 0.9\ \text{s})$, whereas that discharged out of it was 7.5 kJ $(= 10\ \text{kW} \times 0.75\ \text{s})$. The difference came from a power loss within the power devices, mainly the conduction loss. The waveform of p in Fig. 17 allows us to estimate the total loss as

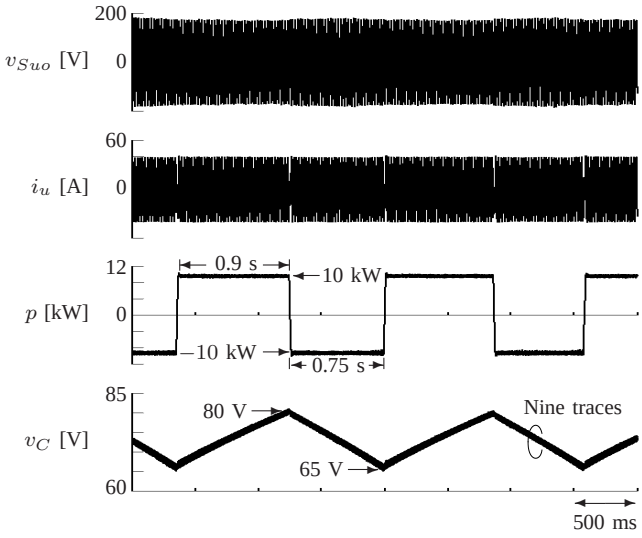

Fig. 17. Experimental waveforms with repetitive charging and discharging of the capacitor bank.

910 W[1]. The conduction loss is calculated to be around 783 W $(= 1.5\ \text{V} \times 29\ \text{A} \times 6 \times 3)$ at 10 kW. The remaining loss $(= 910\ \text{W} - 783\ \text{W})$ consists of a total copper and iron loss in the three ac inductors, and a switching loss that is small due to the dc voltage as low as 65-80 V and the switching frequency as low as 1 kHz.

In contrast to the conduction loss of 783 W (7.8% of 10 kW), the 6.6-kV, 1-MW system with a cascade number of $N = 10$, will have a conduction loss of 10.5 kW $(= 2\ \text{V} \times 87.5\ \text{A} \times 20 \times 3)$ which is only 1% of the rated power, assuming the use of 1.2-kV IGBTs. Since the use of switching frequency as low as 1 kHz also results in reduced switching loss, the 6.6-kV system is expected to reach an overall efficiency of higher than 98%, including the loss in the three ac inductors.

B. Start-up Procedure

The energy storage system requires neither an external starting nor a pre-charging circuit. Fig. 2 includes a simple start-up circuit consisting of a three-phase circuit breaker CB, a three-phase magnetic contactor MC, and a current-limiting resistor R in each phase. Fig. 18 depicts the waveforms during starting up the energy storage system. At the time of $t = 0$, the CB was switched on, while the MC remained switched off. The capacitor bank started charging through the current-limiting resistors R, keeping each converter cell operated as a diode rectifier. The inrush current was limited to 13 A (peak), which was below the rated current of 30 A. At the time of $t = 30$ s, when the starting current decayed to zero, the MC was turned on. The controller was started at the time of $t = 60$ s, and the gate signals were provided to the nine converter cells, along with the active-power command p^*. The controller gradually built up each dc-capacitor voltage to an

[1]The total power loss is given by $1.5^{\text{kJ}}/1.65^{\text{s}}$, where the numerator is the total energy loss $(= 9^{\text{kJ}} - 7.5^{\text{kJ}})$ during one cycle of charging and discharging, and the denominator is the time period of that cycle.

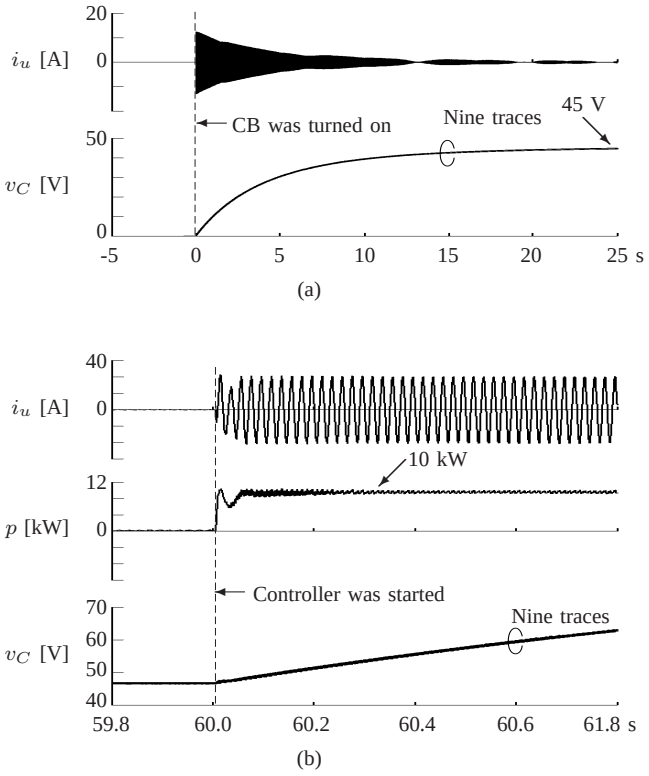

Fig. 18. Experimental waveforms when the energy storage system was started: (a) -5 s $\leq t \leq$ 25 s; (b) 59.8 $\leq t \leq$ 60.8 s.

operating range of 65 to 80 V. Then, the system came into normal operation.

C. Effectiveness of Voltage-Balancing Control

Fig. 19 shows the experimental waveforms when the clustered balancing control was intentionally disabled for about 60 s. Note that the individual balancing was still kept active. The nine capacitor-voltage waveforms look like three traces because all the three dc voltages in a cluster were equal to their dc mean voltage in the corresponding cluster. However, the three dc mean voltages in the three clusters were deviated from the overall dc mean voltage. The clustered balancing control can avoid this situation. The dc-voltage waveforms in Figs. 13-17 conclude that the voltage-balancing controller is effective in balancing all the nine dc voltages.

The capacitance value of the dc capacitor in the first converter cell of the u-phase cluster, C_{u1} was intentionally increased from 0.9 F to 1.1 F by 22%, to further verify the effectiveness of the voltage balancing control. Note that this capacitance imbalance is very rare in an actual system because it is beyond a general capacitance tolerance. Fig. 20 (a) shows that the capacitance imbalance made v_{Cu1} rise up slowly, compared to the other eight voltages $v_{Cu2} \sim v_{Cw3}$, when the system was started. Fig. 20 (b) shows that the voltage-balancing control was effective in keeping all the nine dc voltages balanced.

Fig. 21 shows the time-expanded waveforms of Fig. 20.

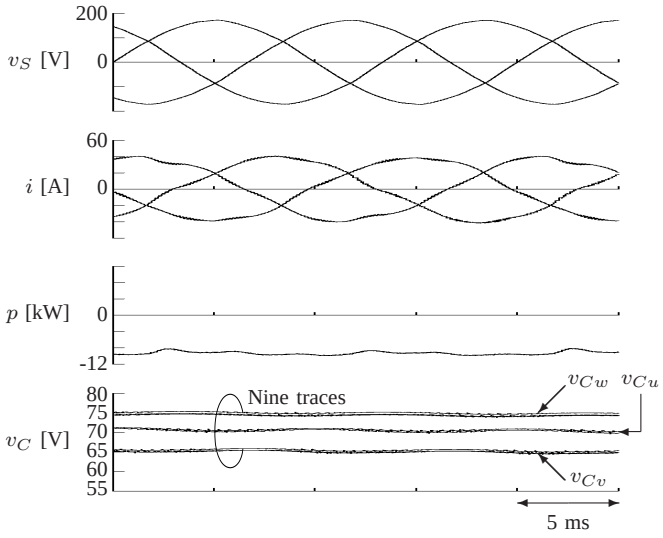

Fig. 19. Experimental waveforms when the clustered balancing control was disabled for about 60 s. The individual balancing control was still kept active in this experiment.

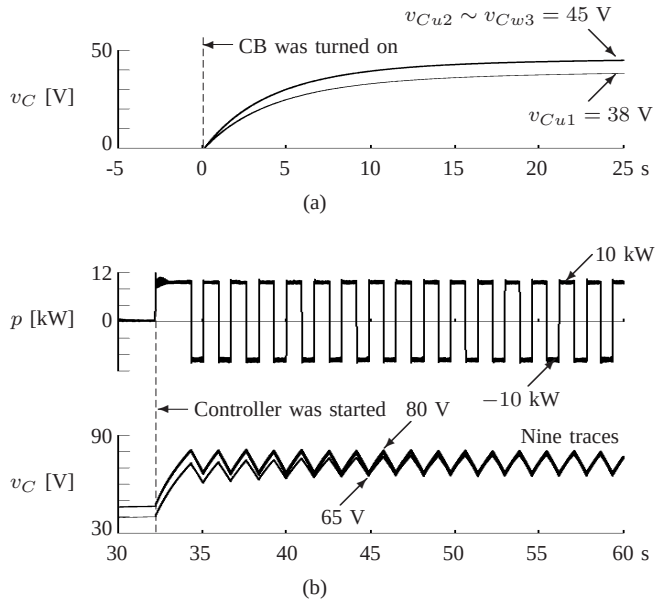

Fig. 20. Experimental waveforms confirming the effectiveness of voltage-balancing control. The capacitance value of C_{u1} was increased from 0.9 F to 1.1 F by 22% in this experiment. (a) -5 s $\leq t \leq$ 25 s, and (b) 30 $\leq t \leq$ 60 s.

VIII. Conclusion

This paper has addressed a 6.6-kV energy storage system without transformers. It is based on cascade connection of several single-phase H-bridge PWM converter cells in each phase. The voltage-balancing control presented in this paper is characterized by stable operation and easy expansion into a higher number of voltage levels. Experimental results obtained from a 200-V, 10-kW, 8.8-kJ laboratory model using electrolytic capacitors have verified the viability of the 6.6-kV transformerless energy storage system.

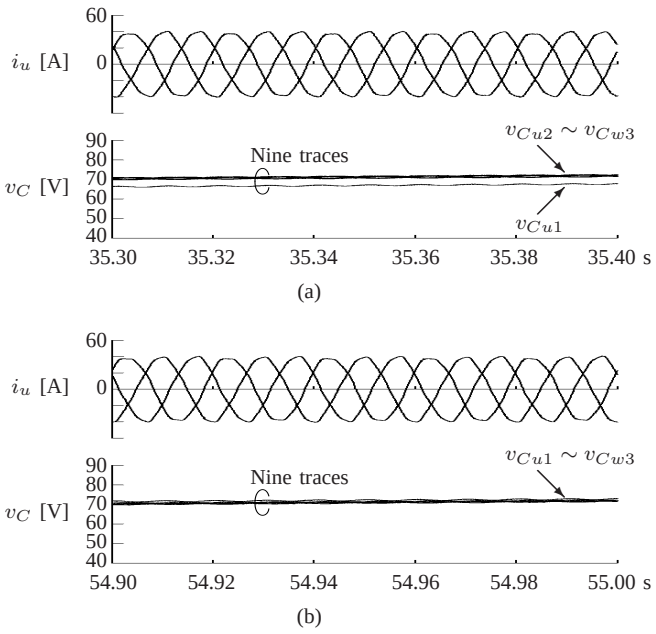

Fig. 21. Time-expanded waveforms of Fig. 20: (a) voltage imbalance appeared, and (b) voltage imbalance disappeared.

REFERENCES

[1] S. M. Halpin, R. L. Spyker, R. M. Nelms, and R. F. Burch, "Application of double-layer capacitor technology to static condensers for distribution system voltage control," *IEEE Trans. Power Sys.*, vol. 11, no. 4, pp. 1899-1904, 1996.

[2] N. W. Miller, R. S. Zrebiec, R. W. Delmerico, and G. Hunt, "Design and commissioning of a 5-MVA, 2.5-MWh battery energy storage," in *Proc. IEEE PES Transmission and Distribution Conf.*, pp. 339-345, 1996.

[3] A. van Zyl, and R. Spee, "Short term energy storage for ASD ride-through," in *Proc. IEEE IAS Annual Meeting*, pp. 1162-1167, 1998.

[4] K. K. Leung, and D. Sutanto, "Using battery energy storage system in a deregulated environment to improve power system performance," in *Proc. Electric Utility Deregulation and Restructuring and Power Technologies Conf. (DRPT2000)*, pp. 614-619, 2000.

[5] Z. Yang, C. shen, L. Zhang, M. L. Crow, and S. Atcitty, "Integration of a STATCOM and battery energy storage," *IEEE Trans. Power Sys.*, vol. 16, no. 2, pp. 254-260, 2001.

[6] A. Arulampalam, J. B. Ekanayake, and N. Jenkins, "Application study of a STATCOM with energy storage," *IEE Proc. Generation, Transmission and Distribution*, vol. 150, no. 3, pp. 373-384, 2003.

[7] D. Casadei, G. Grandi, and C. Rossi, "Power quality and reliability supply improvement using a power conditioning system with energy storage capability," in *Proc. IEEE ISIE*, pp. 1135-1140, 2004.

[8] T. Kinjo, T. Senjyu, N. Urasaki, and H. Fujita, "Output levelling of renewable energy by electric double-layer capacitor applied for energy storage system," *IEEE Trans. Energy Conversion*, vol. 21, no. 1, pp. 221-227, 2006.

[9] J. M. Carrasco, L. G. Franquelo, J. T. Bialasiewicz, E. Galvan, R. C. PortilloGuisado, and M. A. M. Prats, "Power-electronic systems for the grid integration of renewable energy sources: a survey," *IEEE Trans. Ind. Electron.*, vol. 53, no. 4, pp. 1002-1016, 2006.

[10] E. Schempp, and W. D. Jackson, "Systems considerations in capacitive energy storage," in *Proc. Intersociety Energy Conversion Engineering Conf.*, vol. 2, pp. 666-671, 1996.

[11] C. A. Vincent, "Lithium batteries," *IEE Review*, vol. 45, no. 2, pp. 65-68, 1999.

[12] P. F. Ribeiro, B. K. Johnson, M. L. Crow, A. Arsoy, and Y. Liu, "Energy storage systems for advanced power applications," *Proceedings of the IEEE*, vol. 89, no. 12, pp. 1744-1756, 2001.

[13] A. Schneuwly, "Charge ahead [ultracapacitor technology and applications]," *Power Engineer*, vol. 19, no. 1, pp. 34-37, 2005.

[14] P. G. Therond, and I. Joly, "Superconducting magnetic energy storage (SMES) for industrial applications–comparison with battery systems," *IEEE Trans. Applied Superconduct.*, vol. 3, no. 1, pp. 250-253, 1993.

[15] V. Karasik, K. Dixon, C. Webber, B. Batchelder, and P. Ribeiro, "SMES for power utility applications: A review of technical and cost considerations," *IEEE Trans. Appl. Superconduct.*, vol. 9, pp. 541-546, June 1999.

[16] D. Casadei, G. Grandi, and C. Rossi, "A supercapacitor-based power conditioning system for power quality improvement and uninterruptible power supply," in *Proc. IEEE ISIE*, pp. 1247-1252, 2002.

[17] C. Han, A. Q. Huang, D. Li, H. Mamath, M. Ingram, and S. Atcitty, "Modeling and design of a transmission ultracapacitor (TUCAP) integrating modular voltage source converter with ultracapacitor energy storage," in *Proc. IEEE APEC*, pp. 1104-1110, 2006.

[18] L. M. Tolbert, F. Z. Peng, and T. G. Habetler, "Multilevel converters for large electric drives," *IEEE Trans. Ind. Appl.*, vol. 35, no. 1, pp. 36-44, 1999.

[19] J. Rodriguez, J. S. Lai, and F. Z. Peng, "Multilevel inverters: a survey of topologies, controls, and applications," *IEEE Trans. Ind. Electron.*, vol. 49, no. 4, pp. 724-738, 2002.

[20] H. Fujita, S. Tominaga, and H. Akagi, "Analysis and design of a dc voltage-controlled static var compensator using quad-series voltage-source inverters," *IEEE Trans. Ind. Appl.*, vol. 32, no. 4, pp. 970-978, 1996.

[21] H. Akagi, S. Inoue, and T. Yoshii, "Control and performance of a medium-voltage transformerless cascade PWM STATCOM with star configuration," *IEEE Trans. Ind. Appl.*, vol. 43, no. 4, pp. 1041-1049, 2007.

[22] H. Akagi, Y. Kanazawa, and A. Nabae, "Instantaneous reactive power compensators comprising switching devices without energy storage components," *IEEE Trans. Ind. Appl.*, vol. 20, no. 3, pp. 625-630, 1984.

[23] H. Akagi, E. H. Watanabe, and M. Aredes, *Instantaneous Power Theory and Applications to Power Conditioning*. IEEE Press, 2007.

Hirofumi Akagi was born in Okayama, Japan, on 19th August 1951. He received the B.S. degree from the Nagoya Institute of Technology, Nagoya, Japan, in 1974, and the M. S. and Ph. D. degrees from the Tokyo Institute of Technology, Tokyo, Japan, in 1976 and 1979, respectively, all in electrical engineering.

In 1979, he was with the Nagaoka University of Technology, Nagaoka, Japan, as an Assistant and then Associate Professor in the department of electrical engineering. In 1987, he was a Visiting Scientist at the Massachusetts Institute of Technology for ten months. From 1991 to 1999, he was a Professor in the department of electrical engineering at Okayama University, Okayama, Japan. From March to August of 1996, he was a Visiting Professor at the University of Wisconsin, Madison and then the Massachusetts Institute of Technology. Since January 2000, he has been a Professor in the department of electrical and electronic engineering at the Tokyo Institute of Technology, Tokyo, Japan.

His research interests include power conversion systems, ac motor drives, active and passive EMI filters, high-frequency resonant-inverters for induction heating and corona discharge treatment processes, and utility applications of power electronics such as active filters for power conditioning, self-commutated BTB systems, and FACTS devices. He has authored or coauthored some 70 IEEE Journal papers, including two invited papers in *Proceedings of the IEEE* in 2001 and 2005. According to Google Scholar, the total citation index for all his papers is more than 4,800. He has made presentations many times as a keynote or invited speaker internationally.

Since January 2007, he has been the President of the IEEE Power Electronics Society (PELS). He was elected as a Fellow of the IEEE in 1996, and a Distinguished Lecturer of the IEEE Industry Applications Society (IAS) and PELS for 1998-1999. He received two IEEE IAS Transactions Prize Paper Awards in 1991 and 2004, and two IEEE PELS Transactions Prize Paper Awards in 1999 and in 2003, nine IEEE IAS Committee Prize Paper Awards, the 2001 IEEE William E. Newell Power Electronics Award, and the 2004 IEEE IAS Outstanding Achievement Award.

He is a recipient of the 2008 IEEE Richard H. Kaufmann Technical Field Award with the following citation: "For pioneering contributions to the theory of instantaneous reactive power ion three-phase circuits, and it applications to power conditioning."